

pubs.acs.org/NanoLett Letter

DNA Origami Voltage Sensors for Transmembrane Potentials with Single-Molecule Sensitivity

Sarah E. Ochmann, Himanshu Joshi, Ece Büber, Henri G. Franquelim, Pierre Stegemann, Barbara Saccà, Ulrich F. Keyser, Aleksei Aksimentiev, and Philip Tinnefeld*



Cite This: Nano Lett. 2021, 21, 8634-8641



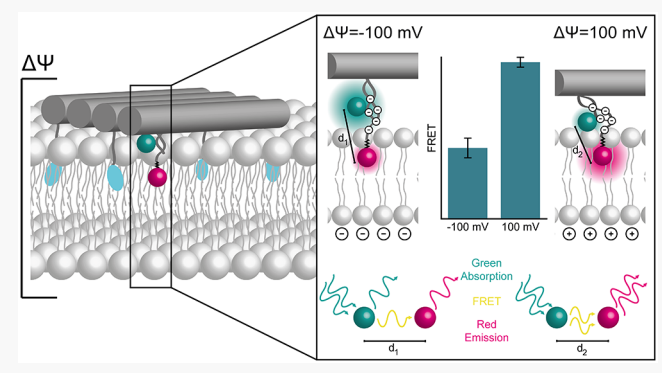
ACCESS

III Metrics & More

Article Recommendations

Supporting Information

ABSTRACT: Signal transmission in neurons goes along with changes in the transmembrane potential. To report them, different approaches, including optical voltage-sensing dyes and genetically encoded voltage indicators, have evolved. Here, we present a DNA nanotechnology-based system and demonstrated its functionality on liposomes. Using DNA origami, we incorporated and optimized different properties such as membrane targeting and voltage sensing modularly. As a sensing unit, we used a hydrophobic red dye anchored to the membrane and an anionic green dye at the DNA to connect the nanostructure and the membrane dye anchor. Voltage-induced displacement of the anionic donor unit was read out by fluorescence resonance energy transfer (FRET) changes of single sensors attached to liposomes. A FRET change of ~5% for



 $\Delta \Psi = 100$ mV was observed. The working mechanism of the sensor was rationalized by molecular dynamics simulations. Our approach holds potential for an application as nongenetically encoded membrane sensors.

KEYWORDS: DNA origami, voltage sensor, single-molecule FRET, transmembrane potential, voltage imaging, molecular dynamic simulations

■ INTRODUCTION

On the cellular level, the electrical transmembrane potential $\Delta\Psi$ is a key parameter in neuroscience. The introduction of fluorescence-based voltage sensors was a milestone toward a broader application and noninvasive visualization in contrast to electrophysiological approaches that are invasive, serial, and time-consuming. Many challenges with respect to signal, contrast, and response time have been addressed with genetically encoded voltage indicators $(\text{GEVIs})^{2-4}$ that offer targetability to cell membranes. For improved contrast and imaging durations, hybrid approaches combining GEVIs with organic fluorophores have been introduced. These approaches, however, require transfected cell lines or transgenic animals.

In contrast, conventional voltage-sensing dyes face the challenge that all functionalities, including targeting membranes and sensing and transducing a signal, have to be encoded in simple, chemically accessible structures. The development of a first generation of sensors yielded low-contrast Stark-effect voltage-sensing dyes and probes that disturbed cellular functions.⁷ A higher contrast was achieved with sensors based on fluorescence energy transfer (FRET), which consisted of one component in the membrane core changing position according to the voltage and a second component on the membrane surface.^{8,9} However, as the

components were not chemically linked, high probe concentrations had to be used, leading to capacitive loading. ¹⁰ Therefore, in recent approaches the complexity of sensors has been increased, including bottom-up nanotechnological ideas, to develop quantum-confined semiconductor nanoparticles or quantum dot—fullerene bioconjugates for voltage sensing. ^{11–13} Recently, DNA was used as a scaffolding material to combine electron-transfer-based voltage-sensing dyes^{7,14,15} with targeting and intensity referencing for voltage sensing in organelles. ¹⁶

In this paper, we used DNA origami to modularly address different challenges of voltage sensor design and demonstrate an alternative voltage-sensing strategy that allows sensing with bright dyes compatible with single-molecule imaging. DNA origami and similar self-assembly techniques offer the potential to meet broad demands such as targeting lipid membranes, incorporating a sensing unit, optionally providing a transduction mechanism with internal referencing, and being biocompatible and minimally invasive.

Received: July 2, 2021
Revised: October 8, 2021
Published: October 18, 2021





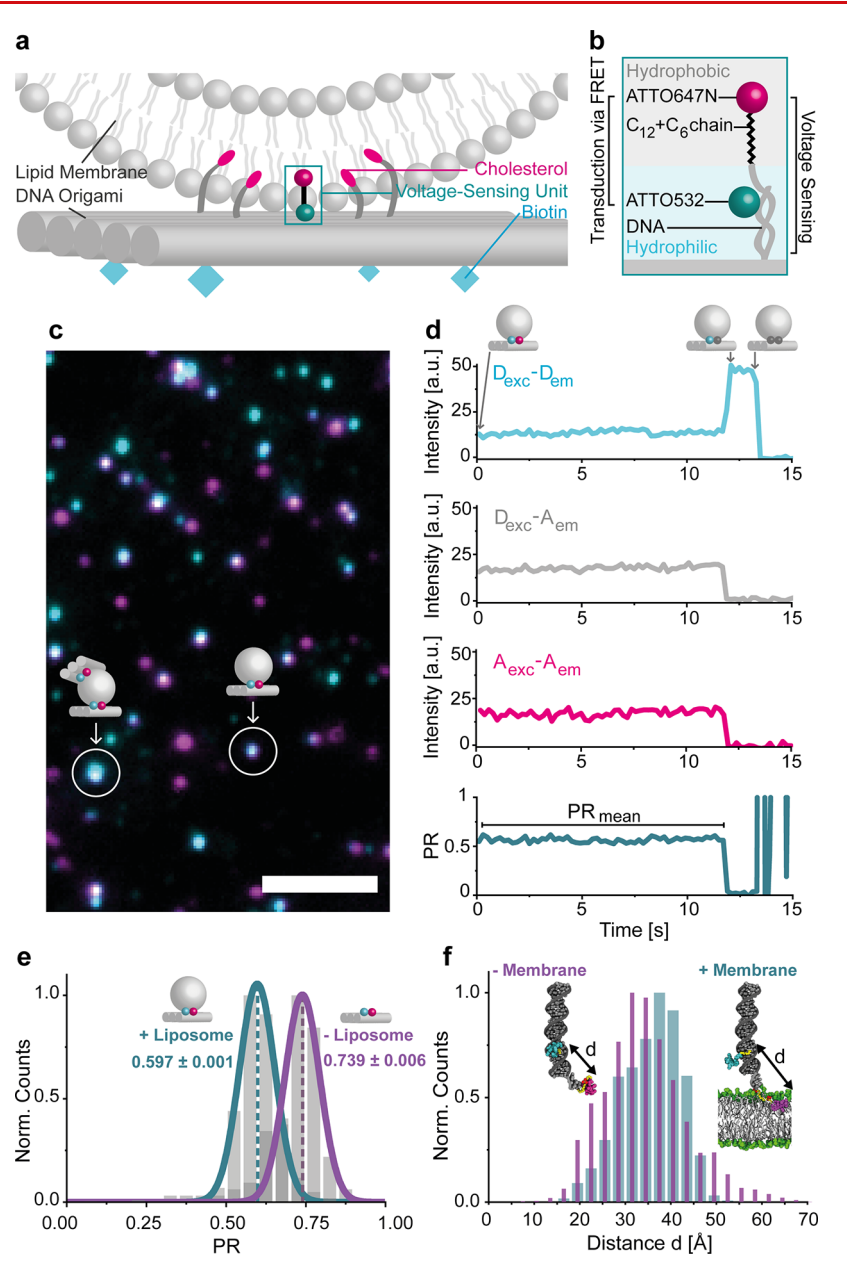


Figure 1. (a) DNA origami sensor of transmembrane potentials. A rectangular DNA origami plate was decorated with cholesterols to bind a liposome and with biotins to attach to the neutravidin-functionalized surface of a microscope's coverslip. The voltage-sensing unit was positioned in the center of the DNA origami. (b) Voltage-sensing unit consisting of dsDNA protruding from the DNA origami plate and carrying an ATTO532 dye and a complementary strand with an ATTO647N dye connected via a C_{12} + C_6 linker (see Figure S2 for the chemical structure). The transduction of the voltage signal to fluorescence was fulfilled by FRET from the donor ATTO532 to the acceptor ATTO647N. (c) Superimposed TIRF image of the donor (blue) and acceptor (pink) fluorescence from the DNA origami sensor. White spots indicate DNA origami plates with both donor and acceptor dyes. The scale bar refers to 5 μm. (d) Single-molecule FRET transient. The fluorescence intensity over time is shown for the donor excitation—donor emission D_{exc} - D_{em} channel (light blue), the donor excitation—acceptor emission D_{exc} - A_{em} channel (gray), and the acceptor excitation—acceptor emission A_{exc} - A_{em} channel (pink). From the D_{exc} - D_{em} and the D_{exc} - D_{em} channels, the proximity ratio (PR) and the PR_{mean} are determined (dark blue). (e) PR distributions for DNA origami constructs with (cyan) and without (purple) the liposome attachment. The error refers to the standard error of the mean. For each sample, $N_{molecule} \ge 100$. (f) Histogram of interdye distances obtained from MD simulations of a dsDNA duplex decorated with the two dyes positioned at the lipid—water interface (cyan) and in an aqueous solution (purple). Simulation times are as follows: −Membrane, 1.35 μ s and +Membrane, 1.55 μ s.

In the DNA origami method, a long single-stranded DNA molecule (ssDNA, > 7000 nucleotides long) is folded into a desired shape by hybridization with short oligonucleotides, producing billions of identical nanostructures. ^{17–19} This bottom-up nanoassembly method offers the ability to place any chemical moiety on the nanostructure like on a molecular breadboard by the integration of modified oligonucleotides.

Using the DNA origami technique, a variety of sensors have been realized, ²⁰ from nanopores ^{21–23} to drug delivery systems ^{24,25} to force sensors. ^{26,27} By capturing DNA origami on nanocapillary tips, Hemmig and Fitzgerald et al. demonstrated the feasibility of using a DNA origami construct as a single-molecule voltage sensor. ²⁸ Two fluorophores capable of interacting via FRET are placed on a DNA

nanostructure such that, when subject to a voltage bias at the tip of a nanopipet, the FRET efficiency is modulated by the voltage magnitude.

Here, we demonstrate the single-molecule transmembrane voltage read-out from the surface of a lipid membrane. Using a rectangular DNA origami to arrange the different components needed, we created a sensor that optically reads out defined potentials via FRET with a change of \sim 5% for $\Delta\Psi$ = 100 mV. FRET offers an advantageous ratiometric signal read-out and is therefore signal intensity independent. We detected single FRET pairs by spacing out origami structures beyond the diffraction limit and hence provide a pathway for imaging at the nanoscale beyond ensemble averages. When a sensor can be detected at the level of single molecules, minimal invasiveness and optical superresolution can be achieved in combination with single-molecule localization-related imaging schemes.^{29,30} We rationalized the functioning of the sensor through molecular dynamics (MD) simulations of the DNAlipid membrane assembly. Further, we demonstrate the potential of DNA nanotechnology for voltage sensing by introducing small molecular changes in the sensing unit to shift the sensitivity of the sensor toward a negative $\Delta\Psi$.

RESULTS

The transmembrane voltage sensor was based on a rectangular DNA origami with dimensions of $70 \times 100 \text{ nm}^{17,31,32}$ that functions as a platform to program all the functionalities required into a small entity. To bind to liposomes, the nanostructure was equipped with ten cholesterol moieties; to bind to biotinylated PLL-e-PEG passivated surfaces, additional six biotin moieties were incorporated (Figures 1a and S1 and Table S1). Surface binding of the liposomes via the DNA origami facilitated imaging by total internal reflection microscopy (TIRF) while avoiding direct surface interactions of the liposomes.³³ The voltage-sensing unit was placed centrally on the platform protruding from the structure. The hydrophobic and cationic dye ATTO647N connected to DNA by a C₁₂-phosphate-C₆ chain (C₁₂+C₆) was expected to anchor the sensor unit in the lipid membrane (see Figures 1b and \$2 for molecular structures). Insertion into the lipid core of the membrane was previously observed for ATTO647N.³⁴ The DNA connection from ATTO647N to the DNA origami platform contained the anionic fluorophore ATTO532. We reasoned that any change of the potential should have opposite effects on the average positions of the cationic ATTO647N dye and the anionic ATTO532 dye on the anionic DNA linker. The opposite forces on the two dyes should translate $\Delta\Psi$ into a change of the FRET that can be read out optically on the level of single molecules.

For imaging, we performed single-molecule FRET (smFRET) experiments of the optical potential sensor on a home-built TIRF microscope with green—red alternating laser excitation (ALEX, for details see the SI). So, We acquired videos to follow the fluorescence over time and verify that single DNA origamis were observed. Figure 1c presents a superimposed TIRF image with donor dyes in blue, acceptor dyes in pink, and an overlay of the two in white. Some of the spots are brighter than others, which is caused by multiple DNA origamis being bound to a single liposome or origami multimers. To eliminate such aggregates in further analysis, we generated intensity-time transients from the videos for each spot with the software iSMS and inspected them visually. An exemplary transient is shown in Figure 1d with $D_{\rm exc}$ — $D_{\rm em}$ (light

blue), $D_{\rm exc}-A_{\rm em}$ (gray), and $A_{\rm exc}-A_{\rm em}$ (pink), where the subscript indicates the excitation and emission channels of the donor (D) and acceptor (A), respectively. A correlated intensity increase in $D_{\rm exc}-D_{\rm em}$ upon an intensity decrease in $D_{\rm exc}-A_{\rm em}$ and $A_{\rm exc}-A_{\rm em}$ and the rapid photobleaching in $D_{\rm exc}-D_{\rm em}$ are clear indications that a single DNA origami indeed was observed. From the intensities $I_{\rm DD}$ of the $D_{\rm exc}-D_{\rm em}$ channel and the intensity $I_{\rm DA}$ of the $D_{\rm exc}-A_{\rm em}$ channel, FRET was quantified as the proximity ratio (PR), where

$$PR = \frac{I_{DA}}{I_{DD} + I_{DA}} \tag{1}$$

The PR_{mean} was calculated over the whole period of the energy transfer (bottom transient in Figure 1d), yielding one data point for each voltage sensor. All single-molecule transients were carefully reviewed, and the ones showing a clear correlation between the three channels mentioned above were picked while transients showing multichromophore behavior were rejected. An exemplary selection of transients is shown in Figures S3 and S4.

We first tested whether an interaction between the voltage sensor and the lipid membrane as intended is detected. To this end, we studied the DNA origamis with and without 100 nm DOPC liposomes by mixing the origami structures with an excess of liposomes and immobilizing the complexes on a surface. After performing smFRET measurements, we obtained PR distributions, as shown in Figure 1e. The liposome-free sample yielded a mean PR of 0.739 ± 0.006 (standard error of the mean, SEM) that was obtained from a Gaussian fitting of the distribution, which decreased to 0.597 \pm 0.001 for the liposome-containing sample (Figure 1e). The fact that we obtained narrow homogeneous populations that were clearly shifted with respect to each other indicates quantitative binding of DNA origami voltage sensors to the liposomes. In addition, the decrease of the FRET supports the idea that the hydrophobic ATTO647N is diving into the membrane core so that the average distance of donor and acceptor is substantially increased upon membrane binding.

We further rationalized the idea of the FRET-acceptor anchoring in the membrane by MD simulations of the voltagesensing unit with and without a lipid membrane present. Figure 1f and Movie S1, provided in the SI, revealed a coiling of ATTO647N with the alkyl chain, resulting in a close proximity of the dyes. This secondary structure was broken in the presence of a lipid membrane (Movie S2) as ATTO647N and the alkyl chain insert to and remain in the hydrophobic core of the membrane. Figure 1f shows the distributions for the interdye distances for both samples that were determined from the MD simulations. The observed shift toward larger distances for the sensor in the presence of a membrane is in good agreement with the experimental results (Figure 1e) and suggests that the lower PR upon liposome addition is a result of the spatial separation of the two dyes. According to Figure S6, the dyes did not show a preferred orientation to each other so that an angular effect on the PR is unlikely. Another interesting observation from the simulations is that the ATTO647N dye remained embedded closest to the membrane and interacted with the phosphate moieties of the lipid head groups (likely because of its positive charge), while the main body of the dye resided inside the hydrophobic core of the membrane.

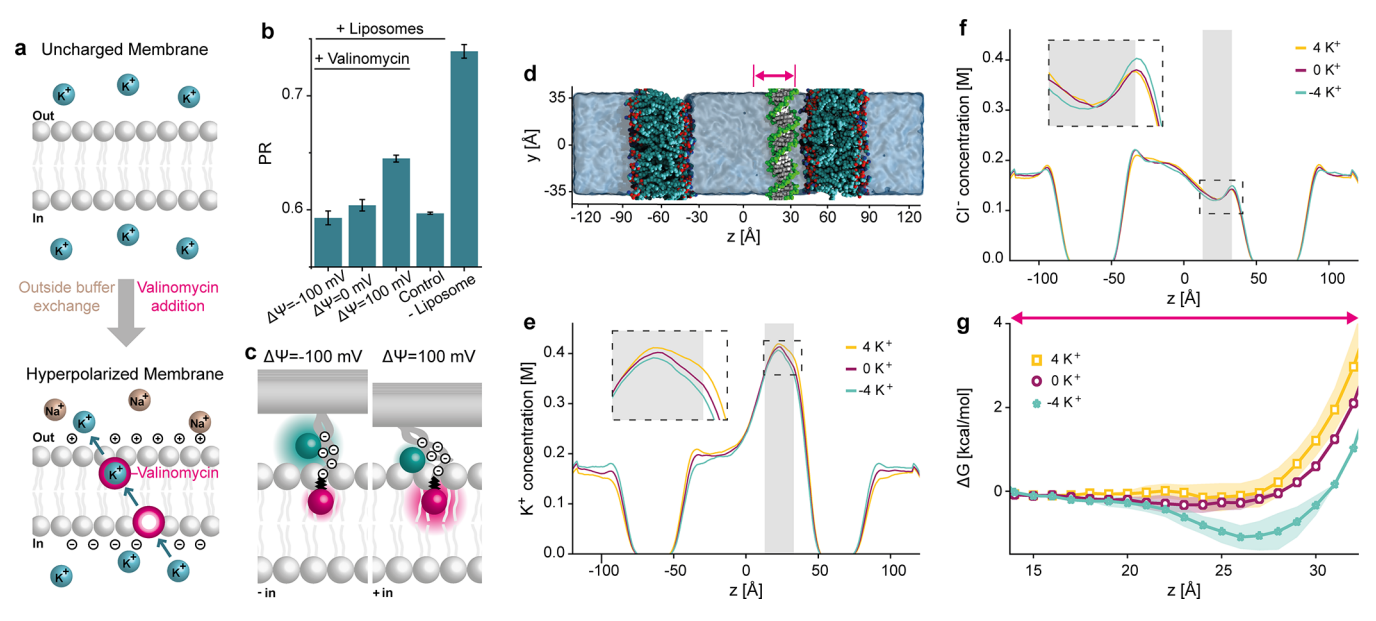


Figure 2. (a) Creation of electrical transmembrane potentials $\Delta\Psi$. By exchanging the outside buffer, a potassium ion gradient across the lipid membrane was built up. Equilibration of the potassium gradient by the ionophore valinomycin converted the chemical potential to an electrical transmembrane potential $\Delta\Psi$. (b) Mean PR and standard errors of the mean derived from Gaussian fits to the distributions (Figures S8 and S9) of the DNA origami—liposome complexes with different $\Delta\Psi$ values in comparison to control samples presented in Figure 1e. For each sample, $N_{\text{molecule}} \geq 100$. (c) Proposed working principle of the voltage-sensing DNA origami. The ATTO647N remains as an anchor in the membrane's hydrophobic core, whereas the surrounding DNA with its anionic nature is attracted toward the membrane by the K⁺ excess inside of the liposome, resulting in a shorter interdye distance and increased FRET. (d) Representative configuration of a simulated double membrane system, where two membrane patches separated two compartments filled with a 150 mM KCl solution. A single dsDNA molecule was placed near one membrane to characterize effective interactions between the DNA and the membrane. A gradient of the K⁺ concentration was established by transferring four K⁺ ions from one compartment to the other, corresponding to a drop of $\Delta\Psi$ = ± 1.3 V. The local concentrations of (e) K⁺ and (f) Cl⁻ ions along the lipid bilayer are shown for the three ion gradient conditions. The z-axis is defined in panel d. The profiles were averaged over 21 replica windows of the respective REUS MD simulations, each replica simulation being 120 ns long. The shaded region shows the location of the center of DNA in various windows. (g) Free energy ΔG of the 21 base pair dsDNA as a function of its z-coordinate for the three ion gradient conditions. The arrow implies the region shown in panel d.

To test the performance of our voltage-sensing DNA origami, we used ion exchange by the ionophore valinomycin 39 to create a well-defined change of $\Delta\Psi$ across the liposome membrane. In a typical experiment, the origami—liposome complexes were imaged, the buffer surrounding was exchanged to introduce a potassium gradient across the lipid membrane, and valinomycin was added before the sample is imaged again (Figure 2a). Valinomycin specifically complexes potassium ions but not sodium ions and shuttles them across the lipid membrane until an equilibrium is reached and a polarized membrane results, following the Nernst equation

$$\Delta \Psi = \frac{RT}{Fz} \ln \left(\frac{c_{\text{in}}^{K^+}}{c_{\text{out}}^{K^+}} \right) \tag{2}$$

where R is the gas constant, T is the temperature, F is the Faraday constant, z is the charge number, and $c_{in}^{K^+}$ and $c_{out}^{K^+}$ are the potassium concentrations inside and outside the liposome, respectively. By adjusting the initial K^+ concentration gradient, we produced a well-defined transmembrane potential (Table S2). Figure S7 confirms the functionality of our assay in bulk experiments using a commercially available voltage-sensing dye.

First, we were interested in three scenarios: a hyperpolarized membrane, a neutral membrane, and a depolarized membrane with respect to the inner leaflet. We chose the hyperpolarization to be $\Delta\Psi=-100$ mV and the depolarization to be $\Delta\Psi=100$ mV, for which the buffer outside was exchanged

with respect to the desired $\Delta\Psi$ and valinomycin was added before imaging. Single Gaussian distributions were obtained for all the samples, and mean PR values of 0.593 \pm 0.006 for $\Delta\Psi$ = -100 mV, 0.604 ± 0.005 for $\Delta \Psi = 0$ mV, and 0.645 ± 0.003 for $\Delta \Psi = 100$ mV were determined (Figures 2b and S8). When compared to that of the liposome-free sample, all the PR values are lower, which in combination with the mono-Gaussian nature of the distributions strongly suggests that the liposomes stayed intact throughout the experimental procedure. As the $\Delta \Psi = 0$ mV sample shows an almost identical PR histogram as the control sample before the valinomycin addition, we are confident that all observed changes in the single-molecule fluorescence result from the $\Delta\Psi$ created and are not from interference with the ionophore (Figures 2b and S9). In contrast, there is a notable increase in the PR for the depolarized membrane compared to those for the hyperpolarized and neutral membranes, which implies that the DNA origami-based sensor is able to report transmembrane potentials on the single-molecule level.

The direction of the FRET change suggests that a more positive charge on the inside would attract the anionic donor dye—DNA hybrid toward the membrane so that FRET would increase (see Figure 2c). An alternative mechanism, where the change of the ion concentration outside the membranes modulates the electrostatic force acting on the dye embedded in the lipid membrane, was ruled out through a set of MD simulations that examined the distribution of the electrostatic potential in a double-membrane system (Figurse S10 and

S11). It has been previously established that the electric potential of the membrane's interior is approximately 500 mV higher than the electric potential of the surrounding electrolyte. A slight imbalance of ion concentration, i.e., a transfer of just one ion between the compartments of our simulated double-membrane system as shown in Figure S10, produced the expected voltage difference between the electrolyte compartments. However, the gradient of the electrostatic potential across the leaflets of the lipid bilayers remained largely unaffected by the ion concentration gradient as most of the additional potential drop occurs at the interface of the lipid head groups and the electrolyte, which is why we ruled out a movement of the membrane-anchored ATTO647N.

To directly probe the effect of an ion concentration gradient on the interaction between DNA and a lipid membrane, we simulated another double-membrane system (Figure 2d) where one DNA molecule was placed near the surface of one of the membranes parallel to the membrane surface. In addition to the system containing two charge-neutral electrolyte compartments (0 K⁺), two variants of the system were created by moving four K⁺ either to (4 K⁺) or from (-4 K⁺) the compartment containing the DNA, which corresponded to $\Delta \Psi = 0$, $\Delta \Psi = +1.3$, and $\Delta \Psi = -1.3$ V, respectively (Figure S11). Such higher than experimental bias conditions were chosen to increase the effective force on the dsDNA, facilitating convergence of the free-energy calculations (described below). Replica exchange umbrella sampling (REUS) simulations 42 were performed for each system using 21 sampling windows (in 1 Å increments) for the distance between the centers of mass of the dsDNA and the nearby membrane along the z-axis. The resulting ion gradient produced the expected $\Delta\Psi$ across the compartments (Figure S11). Further, the local concentrations of K+ (Figure 2e) and Cl⁻ (Figure 2f) ions show a nontrivial behavior. In the profiles for all three samples, it is clearly visible that the K+ concentration was higher close to the DNA while the Clconcentration was lower, which is due to the electrostatic attraction and repulsion to the anionic DNA backbone, respectively. In the case of an excess of K⁺ ions inside (4 K⁺), the K⁺ concentration was also higher close to the inner leaflets. Interestingly, the concentration at the respective outer leaflets was lower, indicating a capacitive effect. The opposite behavior was observed for the lack of K^+ ions inside $(-4 K^+)$. A complementary effect was observed for the Cl⁻ concentration (Figure 2f).

Further analysis of the REUS simulations yields the free energy of the dsDNA as a function of its proximity to the lipid membrane (Figure 2g). In the absence of a K⁺ gradient, the free energy has a shallow minimum near the membrane surface, which is in agreement with our previous calculations. Moving the positive charge across the membrane from the compartment housing (-4 K⁺ trace) produced a free-energy minimum near the membrane surface, promoting DNA attraction to the membrane surface. Moving the positive charge into the DNA compartment (4 K⁺ trace) slightly increased the repulsive interaction between DNA and the lipid membrane. These simulation results are in a qualitative agreement with our observation of a FRET increase for depolarized membranes and support the mechanism shown in Figure 2c.

Next, we studied the sensitivity of our voltage sensor in more detail and varied the potentials from $\Delta\Psi=-125~mV$ to $\Delta\Psi=125~mV$ in steps of 25 mV. For each sample, the mean

PR before creating $\Delta\Psi$ was approximately the same (Figure S12). We therefore merged all reference data and defined it as the mean of the control sample PR_{before}. This value was subtracted from the PR after $\Delta\Psi$ was built up (Figure S8) as

$$\Delta PR = PR - PR_{before} \tag{3}$$

to yield the change ΔPR . The respective SEM was derived after Gaussian error propagation (see the SI), and the data are presented in Figure 3. In accordance with the results discussed

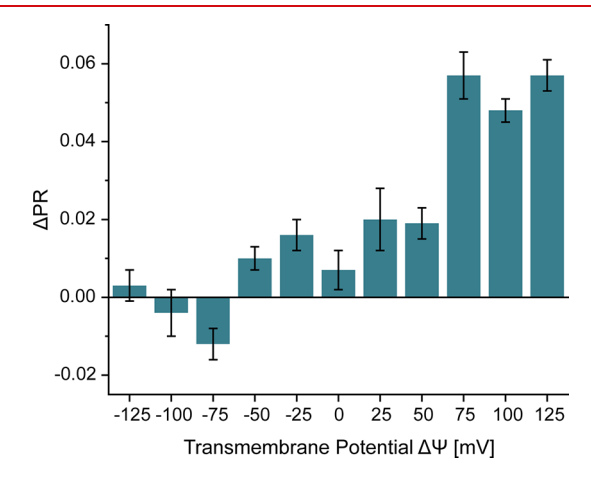


Figure 3. Changes $\Delta \rm PR$ of the voltage sensor exposed to liposomes with different electrical transmembrane potentials $\Delta \Psi.$ $\Delta \rm PR$ was calculated by subtracting the mean PR before the potentials $\Delta \Psi$ were created from the respective PR of the sample, as indicated. The error bars represent the standard error of the mean after Gaussian error propagation. For each sample, $N_{\rm molecule}=100.$

above, the PR value only slightly increased up to $\Delta\Psi=50~mV$ and increased strongly in the range from 50 to 100 mV. The voltage sensor is thus able to transduce small changes in $\Delta\Psi$ to single-molecule fluorescence signals. The nonlinear response might indicate that the sensing unit above the membrane did not progressively shift in the changing $\Delta\Psi$ but that more specific conformational changes or displacements of the dyes occurred.

As our proposed mechanism strongly relies on the relative positioning of the donor dye with respect to the acceptor dye, we checked the sensitivity of the system for small changes of the linker. We therefore changed the voltage-sensing unit minimally by shortening the carbon chain from a $C_{12}+C_6$ to a C₁₂ chain, also eliminating the additional phosphate group (Figure 4a, for details see Figure S2). Interestingly, in the absence of the liposomes the PR was only minimally higher for the shorter linker (PR = 0.754 instead of 0.739). Upon binding to the liposome, however, the PR did only slightly decrease to PR = 0.732 for the shorter linker, indicating that stretching of the hydrophobic linker is mainly responsible for the FRET reduction in case of the $C_{12}+C_6$ linker (Figures S13 and S14). Varying the transmembrane potential of the liposomes exposed to the DNA origami voltage sensor with the shortened linker had an interesting effect on the measured PR values. Most of the signal change now occurred in the more physiologically relevant range between -100 and 0 mV, whereas only a small PR increase was detected for positive $\Delta\Psi$ (Figures 4b, S14, and S15). The direction of change is compatible with the idea that the FRET reduction is not a linear displacement in the $\Delta\Psi$ but instead is related to a more specific conformational change. As the DNA and the negatively charged dye are pulled

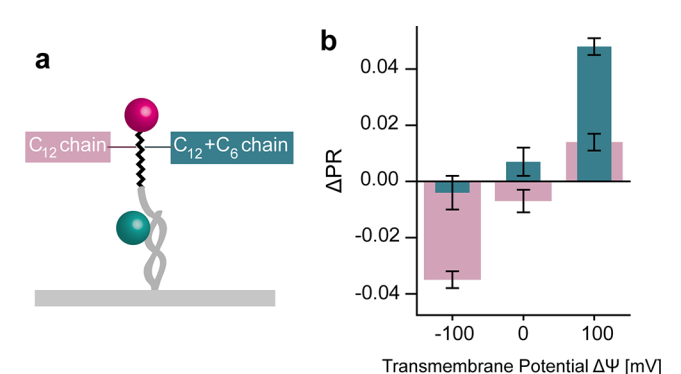


Figure 4. (a) Voltage sensing unit with a C_{12} chain (pink) and a C_{12} + C_6 chain (blue). (b) ΔPR changes of the sensor with a C_{12} chain (pink) in the voltage-sensing unit illustrated in panel a exposed to liposomes with ΔΨ= −100, 0, and 100 mV compared to the voltage-sensing unit with a C_{12} + C_6 chain (blue). ΔPR was estimated by subtracting the mean PR before of the potentials were created from the respective PR of the sample, as indicated. The error bars represent the standard error of the mean after Gaussian error propagation. For each sample, $N_{\text{molecule}} \ge 91$ for each sample.

toward the membrane by the shorter linker, a more negative potential is required to displace them from the membrane so that the FRET reduction occurs. To prove that the sensing mechanism is reversible, we performed an experiment in which the potential was destroyed by ion channels in the membrane. The data in Figures S16 and S17 show a recovery of the PR signal.

CONCLUSION

Transmembrane potentials are key parameters to understand cellular functions and interactions, and there is a great need for the development of smart sensing systems. We here present a DNA origami voltage sensor offering a robust platform to include many functionalities, such as surface immobilization and liposome binding. DNA origami applications in live-cell experiments have been established, and DNA origami stabilization strategies 44-46 such as those against nucleases exist that could be tested for their compatibility with the sensor functionality. The DNA origami nanotech platform could then be extended by further smart functionalities, including specific cell or organelle recognition or for immune system camouflage. 44,47,48

We also introduced a new sensing unit that is based on FRET between a hydrophobic dye that preferred a location in the hydrophobic membrane core and a hydrophilic and anionic dye—DNA moiety that reacted with a PR change of $\sim\!5\%$ for $\Delta\Psi=100$ mV. The DNA origami voltage sensors were studied by single-molecule spectroscopy on liposomes, and the results were rationalized by MD simulations. While the fundamental working principle is implied by the experimental results, the MD simulations provide evidence that more specific interactions between the membrane and the sensing unit determine the sensitive voltage range that could be tuned by the adaptation of the linker between donor and acceptor. Overall, our data show profound potential for this novel approach for $\Delta\Psi$ sensors that could similarly be adapted for other sorts of sensors.

ASSOCIATED CONTENT

Supporting Information

The Supporting Information is available free of charge at https://pubs.acs.org/doi/10.1021/acs.nanolett.1c02584.

Materials and methods, illustration of the DNA origami design, DNA oligonucleotides used as staple strands, detailed sketch of the voltage-sensor designs, exmplary fluorescence transients, equilibrium MD simulation of dye-conjugated dsDNA in aqueous and membrane-anchored environments, angle distributions, concentration of KCl and NaCl in the buffer inside and outside of the LUVs, valinomycin bulk test, PR distributions, voltage bias, average electrostatic profiles, reversibility experiment for the $\rm C_{12}$ sensor, and captions to the supplementary movies (PDF)

All-atom MD simulation of dyes on dsDNA (MP4) All-atom MD simulation of dyes on dsDNA with a lipid membrane (MP4)

mrDNA simulation of the DNA origami (MP4)

AUTHOR INFORMATION

Corresponding Author

Philip Tinnefeld — Department of Chemistry and Center for NanoScience, Ludwig-Maximilians-Universität München, 81377 München, Germany; orcid.org/0000-0003-4290-7770; Email: philip.tinnefeld@cup.uni-muenchen.de

Authors

Sarah E. Ochmann – Department of Chemistry and Center for NanoScience, Ludwig-Maximilians-Universität München, 81377 München, Germany; orcid.org/0000-0002-7553-4600

Himanshu Joshi — Department of Physics and Beckman Institute for Advanced Science and Technology, University of Illinois, Urbana, Illinois 61820, United States; orcid.org/ 0000-0003-0769-524X

Ece Büber – Department of Chemistry and Center for NanoScience, Ludwig-Maximilians-Universität München, 81377 München, Germany

Henri G. Franquelim – Max Planck Institute of Biochemistry, 82152 Planegg, Germany; orcid.org/0000-0001-6229-4276

Pierre Stegemann – Center of Medical Biotechnology (ZMB) and Center for Nano Integration Duisburg-Essen (CENIDE), University of Duisburg—Essen, 45117 Essen, Germany

Barbara Saccà — Center of Medical Biotechnology (ZMB) and Center for Nano Integration Duisburg-Essen (CENIDE), University of Duisburg—Essen, 45117 Essen, Germany; orcid.org/0000-0003-2708-2272

Ulrich F. Keyser – Cavendish Laboratory, Department of Physics, University of Cambridge, Cambridge CB3 0HE, United Kingdom; ⊚ orcid.org/0000-0003-3188-5414

Aleksei Aksimentiev — Department of Physics and Beckman Institute for Advanced Science and Technology, University of Illinois, Urbana, Illinois 61820, United States; orcid.org/0000-0002-6042-8442

Complete contact information is available at: https://pubs.acs.org/10.1021/acs.nanolett.1c02584

Funaing

Deutsche Forschungsgemeinschaft (DFG) (Grants INST 86/1904-1 FUGG and TI 329/10-1 and Project SFB1032 (ID

201269156)), the National Science Foundation (USA) (DMR-1827346), an XSEDE allocation Grant (MCA05S028), and the Leadership Resource Allocation (MCB20012).

Notes

The authors declare no competing financial interest.

ACKNOWLEDGMENTS

A.A. and H.J. would like to thank Christopher Maffeo for his help in setting up the initial mrDNA simulation.

ABBREVIATIONS

GEVI, Genetically-Encoded Voltage Indicator; FRET, Fluorescence Resonance Energy Transfer; ssDNA, Single-Stranded DNA; MD, Molecular Dynamic; TIRF, Total Internal Reflection Fluorescence; dsDNA, Double-Stranded DNA; smFRET, Single-Molecule FRET; ALEX, Alternating Laser Excitation; PR, Proximity Ratio; SEM, Standard Error of the Mean; REUS, Replica Exchange Umbrella Sampling

REFERENCES

- (1) Sepehri Rad, M.; Choi, Y.; Cohen, L. B.; Baker, B. J.; Zhong, S.; Storace, D. A.; Braubach, O. R. Voltage and Calcium Imaging of Brain Activity. *Biophys. J.* **2017**, *113* (10), 2160–2167.
- (2) Platisa, J.; Pieribone, V. A. Genetically encoded fluorescent voltage indicators: Are we there yet? *Curr. Opin. Neurobiol.* **2018**, *50*, 146–153.
- (3) Adam, Y.; Kim, J. J.; Lou, S.; Zhao, Y.; Xie, M. E.; Brinks, D.; Wu, H.; Mostajo-Radji, M. A.; Kheifets, S.; Parot, V.; Chettih, S.; Williams, K. J.; Gmeiner, B.; Farhi, S. L.; Madisen, L.; Buchanan, E. K.; Kinsella, I.; Zhou, D.; Paninski, L.; Harvey, C. D.; Zeng, H.; Arlotta, P.; Campbell, R. E.; Cohen, A. E. Voltage imaging and optogenetics reveal behaviour-dependent changes in hippocampal dynamics. *Nature* **2019**, *569* (7756), 413–417.
- (4) Ma, Y.; Yamamoto, Y.; Nicovich, P. R.; Goyette, J.; Rossy, J.; Gooding, J. J.; Gaus, K. A FRET sensor enables quantitative measurements of membrane charges in live cells. *Nat. Biotechnol.* **2017**, *35* (4), 363–370.
- (5) Chanda, B.; Blunck, R.; Faria, L. C.; Schweizer, F. E.; Mody, I.; Bezanilla, F. A hybrid approach to measuring electrical activity in genetically specified neurons. *Nat. Neurosci.* **2005**, 8 (11), 1619–1626.
- (6) Abdelfattah, A. S.; Kawashima, T.; Singh, A.; Novak, O.; Liu, H.; Shuai, Y.; Huang, Y.-C.; Campagnola, L.; Seeman, S. C.; Yu, J.; Zheng, J.; Grimm, J. B.; Patel, R.; Friedrich, J.; Mensh, B. D.; Paninski, L.; Macklin, J. J.; Murphy, G. J.; Podgorski, K.; Lin, B.-J.; Chen, T.-W.; Turner, G. C.; Liu, Z.; Koyama, M.; Svoboda, K.; Ahrens, M. B.; Lavis, L. D.; Schreiter, E. R. Bright and photostable chemigenetic indicators for extended in vivo voltage imaging. *Science* 2019, 365 (6454), 699–704.
- (7) Miller, E. W.; Lin, J. Y.; Frady, E. P.; Steinbach, P. A.; Kristan, W. B.; Tsien, R. Y. Optically monitoring voltage in neurons by photo-induced electron transfer through molecular wires. *Proc. Natl. Acad. Sci. U. S. A.* **2012**, *109* (6), 2114–2119.
- (8) González, J. E.; Tsien, R. Y. Voltage sensing by fluorescence resonance energy transfer in single cells. *Biophys. J.* **1995**, *69* (4), 1272–1280.
- (9) González, J. E.; Tsien, R. Y. Improved indicators of cell membrane potential that use fluorescence resonance energy transfer. *Chem. Biol.* **1997**, 4 (4), 269–277.
- (10) Miller, E. W. Small molecule fluorescent voltage indicators for studying membrane potential. *Curr. Opin. Chem. Biol.* **2016**, *33*, 74–80
- (11) Nag, O. K.; Stewart, M. H.; Deschamps, J. R.; Susumu, K.; Oh, E.; Tsytsarev, V.; Tang, Q.; Efros, A. L.; Vaxenburg, R.; Black, B. J.; Chen, Y.; O'Shaughnessy, T. J.; North, S. H.; Field, L. D.; Dawson, P. E.; Pancrazio, J. J.; Medintz, I. L.; Chen, Y.; Erzurumlu, R. S.; Huston,

- A. L.; Delehanty, J. B. Quantum Dot-Peptide-Fullerene Bioconjugates for Visualization of in Vitro and in Vivo Cellular Membrane Potential. *ACS Nano* **2017**, *11* (6), 5598–5613.
- (12) Park, K.; Kuo, Y.; Shvadchak, V.; Ingargiola, A.; Dai, X.; Hsiung, L.; Kim, W.; Zhou, H.; Zou, P.; Levine, A. J.; Li, J.; Weiss, S. Membrane insertion of-and membrane potential sensing by-semi-conductor voltage nanosensors:Feasibility demonstration. *Sci. Adv.* **2018**, *4* (1), No. e1601453.
- (13) Liu, J.; Zhang, R.; Shang, C.; Zhang, Y.; Feng, Y.; Pan, L.; Xu, B.; Hyeon, T.; Bu, W.; Shi, J.; Du, J. Near-Infrared Voltage Nanosensors Enable Real-Time Imaging of Neuronal Activities in Mice and Zebrafish. J. Am. Chem. Soc. 2020, 142 (17), 7858–7867.
- (14) Klymchenko, A. S.; Stoeckel, H.; Takeda, K.; Mély, Y. Fluorescent probe based on intramolecular proton transfer for fast ratiometric measurement of cellular transmembrane potential. *J. Phys. Chem. B* **2006**, *110* (27), 13624–13632.
- (15) Nag, O. K.; Jeong, J.-E.; Le, V. S.; Oh, E.; Woo, H. Y.; Delehanty, J. B. Anionic Conjugated Polyelectrolytes for FRET-based Imaging of Cellular Membrane Potential. *Photochem. Photobiol.* **2020**, 96 (4), 834–844.
- (16) Saminathan, A.; Devany, J.; Veetil, A. T.; Suresh, B.; Pillai, K. S.; Schwake, M.; Krishnan, Y. A DNA-based voltmeter for organelles. *Nat. Nanotechnol.* **2021**, *16* (1), 96–103.
- (17) Rothemund, P. W. K. Folding DNA to create nanoscale shapes and patterns. *Nature* **2006**, 440 (7082), 297–302.
- (18) Douglas, S. M.; Dietz, H.; Liedl, T.; Högberg, B.; Graf, F.; Shih, W. M. Self-assembly of DNA into nanoscale three-dimensional shapes. *Nature* **2009**, *459* (7245), 414–418.
- (19) Douglas, S. M.; Marblestone, A. H.; Teerapittayanon, S.; Vazquez, A.; Church, G. M.; Shih, W. M. Rapid prototyping of 3D DNA-origami shapes with caDNAno. *Nucleic Acids Res.* **2009**, 37 (15), 5001–5006.
- (20) Shen, L.; Wang, P.; Ke, Y. DNA Nanotechnology-Based Biosensors and Therapeutics. *Adv. Healthcare Mater.* **2021**, *10* (15), No. 2002205.
- (21) Wei, R.; Martin, T. G.; Rant, U.; Dietz, H. DNA origami gatekeepers for solid-state nanopores. *Angew. Chem., Int. Ed.* **2012**, *51* (20), 4864–4867.
- (22) Hernández-Ainsa, S.; Bell, N. A. W.; Thacker, V. V.; Göpfrich, K.; Misiunas, K.; Fuentes-Perez, M. E.; Moreno-Herrero, F.; Keyser, U. F. DNA origami nanopores for controlling DNA translocation. *ACS Nano* **2013**, *7* (7), 6024–6030.
- (23) Thomsen, R. P.; Malle, M. G.; Okholm, A. H.; Krishnan, S.; Bohr, S. S.-R.; Sørensen, R. S.; Ries, O.; Vogel, S.; Simmel, F. C.; Hatzakis, N. S.; Kjems, J. A large size-selective DNA nanopore with sensing applications. *Nat. Commun.* **2019**, *10* (1), 5655.
- (24) Jiang, Q.; Song, C.; Nangreave, J.; Liu, X.; Lin, L.; Qiu, D.; Wang, Z.-G.; Zou, G.; Liang, X.; Yan, H.; Ding, B. DNA origami as a carrier for circumvention of drug resistance. *J. Am. Chem. Soc.* **2012**, 134 (32), 13396–13403.
- (25) Zhang, Q.; Jiang, Q.; Li, N.; Dai, L.; Liu, Q.; Song, L.; Wang, J.; Li, Y.; Tian, J.; Ding, B.; Du, Y. DNA origami as an in vivo drug delivery vehicle for cancer therapy. ACS Nano 2014, 8 (7), 6633–6643.
- (26) Nickels, P. C.; Wünsch, B.; Holzmeister, P.; Bae, W.; Kneer, L. M.; Grohmann, D.; Tinnefeld, P.; Liedl, T. Molecular force spectroscopy with a DNA origami-based nanoscopic force clamp. *Science* **2016**, 354 (6310), 305–307.
- (27) Kramm, K.; Schröder, T.; Gouge, J.; Vera, A. M.; Gupta, K.; Heiss, F. B.; Liedl, T.; Engel, C.; Berger, I.; Vannini, A.; Tinnefeld, P.; Grohmann, D. DNA origami-based single-molecule force spectroscopy elucidates RNA Polymerase III pre-initiation complex stability. *Nat. Commun.* **2020**, *11* (1), 2828.
- (28) Hemmig, E. A.; Fitzgerald, C.; Maffeo, C.; Hecker, L.; Ochmann, S. E.; Aksimentiev, A.; Tinnefeld, P.; Keyser, U. F. Optical Voltage Sensing Using DNA Origami. *Nano Lett.* **2018**, *18* (3), 1962–1971.
- (29) Weiss, S. Fluorescence spectroscopy of single biomolecules. *Science* **1999**, 283 (5408), 1676–1683.

- (30) Tinnefeld, P.; Sauer, M. Branching out of single-molecule fluorescence spectroscopy: challenges for chemistry and influence on biology. *Angew. Chem., Int. Ed.* **2005**, 44 (18), 2642–2671.
- (31) Woo, S.; Rothemund, P. W. K. Programmable molecular recognition based on the geometry of DNA nanostructures. *Nat. Chem.* **2011**, 3 (8), 620–627.
- (32) Schmied, J. J.; Gietl, A.; Holzmeister, P.; Forthmann, C.; Steinhauer, C.; Dammeyer, T.; Tinnefeld, P. Fluorescence and superresolution standards based on DNA origami. *Nat. Methods* **2012**, *9* (12), 1133–1134.
- (33) Gietl, A.; Holzmeister, P.; Grohmann, D.; Tinnefeld, P. DNA origami as biocompatible surface to match single-molecule and ensemble experiments. *Nucleic Acids Res.* **2012**, *40* (14), No. e110.
- (34) Mobarak, E.; Javanainen, M.; Kulig, W.; Honigmann, A.; Sezgin, E.; Aho, N.; Eggeling, C.; Rog, T.; Vattulainen, I. How to minimize dye-induced perturbations while studying biomembrane structure and dynamics:PEG linkers as a rational alternative. *Biochim. Biophys. Acta, Biomembr.* **2018**, *1860* (11), 2436–2445.
- (35) Ha, T.; Enderle, T.; Ogletree, D. F.; Chemla, D. S.; Selvin, P. R.; Weiss, S. Probing the interaction between two single molecules:Fluorescence resonance energy transfer between a single donor and a single acceptor. *Proc. Natl. Acad. Sci. U. S. A.* 1996, 93 (13), 6264–6268.
- (36) Kapanidis, A. N.; Lee, N. K.; Laurence, T. A.; Doose, S.; Margeat, E.; Weiss, S. Fluorescence-aided molecule sorting: Analysis of structure and interactions by alternating-laser excitation of single molecules. *Proc. Natl. Acad. Sci. U. S. A.* **2004**, *101* (24), 8936–8941.
- (37) Margeat, E.; Kapanidis, A. N.; Tinnefeld, P.; Wang, Y.; Mukhopadhyay, J.; Ebright, R. H.; Weiss, S. Direct observation of abortive initiation and promoter escape within single immobilized transcription complexes. *Biophys. J.* **2006**, *90* (4), 1419–1431.
- (38) Preus, S.; Noer, S. L.; Hildebrandt, L. L.; Gudnason, D.; Birkedal, V. iSMS:Single-molecule FRET microscopy software. *Nat. Methods* **2015**, *12* (7), 593–594.
- (39) Hope, M. J.; Bally, M. B.; Webb, G.; Cullis, P. R. Production of large unilamellar vesicles by a rapid extrusion procedure. Characterization of size distribution, trapped volume and ability to maintain a membrane potential. *Biochim. Biophys. Acta, Biomembr.* **1985**, 812 (1), 55–65.
- (40) Cheng, J.-X.; Pautot, S.; Weitz, D. A.; Xie, X. S. Ordering of water molecules between phospholipid bilayers visualized by coherent anti-Stokes Raman scattering microscopy. *Proc. Natl. Acad. Sci. U. S. A.* **2003**, *100* (17), 9826–9830.
- (41) Aksimentiev, A.; Schulten, K. Imaging alpha-hemolysin with molecular dynamics:Ionic conductance, osmotic permeability, and the electrostatic potential map. *Biophys. J.* **2005**, *88* (6), 3745–3761.
- (42) Sugita, Y.; Kitao, A.; Okamoto, Y. Multidimensional replica-exchange method for free-energy calculations. *J. Chem. Phys.* **2000**, 113 (15), 6042–6051.
- (43) Morzy, D.; Rubio-Sánchez, R.; Joshi, H.; Aksimentiev, A.; Di Michele, L.; Keyser, U. F. Cations Regulate Membrane Attachment and Functionality of DNA Nanostructures. *J. Am. Chem. Soc.* **2021**, 143 (19), 7358–7367.
- (44) Douglas, S. M.; Bachelet, I.; Church, G. M. A logic-gated nanorobot for targeted transport of molecular payloads. *Science* **2012**, 335 (6070), 831–834.
- (45) Keller, A.; Linko, V. Challenges and Perspectives of DNA Nanostructures in Biomedicine. *Angew. Chem., Int. Ed.* **2020**, *59* (37), 15818–15833.
- (46) Chandrasekaran, A. R. Nuclease resistance of DNA nanostructures. *Nat. Rev. Chem.* **2021**, *5*, 225–239.
- (47) Amir, Y.; Ben-Ishay, E.; Levner, D.; Ittah, S.; Abu-Horowitz, A.; Bachelet, I. Universal computing by DNA origami robots in a living animal. *Nat. Nanotechnol.* **2014**, *9* (5), 353–357.
- (48) Li, S.; Jiang, Q.; Liu, S.; Zhang, Y.; Tian, Y.; Song, C.; Wang, J.; Zou, Y.; Anderson, G. J.; Han, J.-Y.; Chang, Y.; Liu, Y.; Zhang, C.; Chen, L.; Zhou, G.; Nie, G.; Yan, H.; Ding, B.; Zhao, Y. A DNA nanorobot functions as a cancer therapeutic in response to a molecular trigger in vivo. *Nat. Biotechnol.* **2018**, *36* (3), 258–264.